remote sensing

MDPI

Article

UAV-Based Deep Learning Workflows for High-Resolution Detection and Mapping of Elkhorn Coral (*Acropora palmata*)

George T. Raber [1,*], Samuel Wyatt [1] and Steven R. Schill [2]

[1] School of Biological, Environmental, and Earth Sciences, The University of Southern Mississippi, Hattiesburg, MS 39406, USA
[2] Caribbean Program, The Nature Conservancy, Christiansted, St. Croix, VI 00820, USA; sschill@tnc.org
* Correspondence: george.raber@usm.edu; Tel.: +1-601-266-4748

Highlights

What are the main findings?

- MaskRCNN deep learning models accurately detect individual *Acropora palmata* colonies from UAwingtrwingtraV-derived orthomosaics with 1.8 cm spatial resolution.
- An iterative annotation refinement strategy, in which initial MaskRCNN outputs were refined and used to augment the training data, markedly improved model overall accuracy.
- Detection accuracy was dependent on colony size and apparent water depth. Colonies wider than approximately 0.3 m and located in shallower water were detected with higher reliability, achieving F1 scores of 0.87 and 0.81, respectively.

What are the implications of the main findings?

- Accurate identification of *A. palmata* relies heavily on resolving colony-level physical structure, which becomes challenging for smaller colonies. Detecting colonies smaller than approximately 0.3 m and distinguishing them from visually similar benthic features will require higher spatial resolution imagery and/or improved signal-to-noise enhancement techniques.
- UAV-derived output of coral locations (MaskRCNN output polygons), enable high-resolution coral density mapping that complements coarser remote sensing products. These outputs provide actionable information for restoration monitoring, population assessments, and conservation decision-making at management-relevant scales.

Abstract

Elkhorn coral (*Acropora palmata*) is a threatened reef-building species that plays a critical role in Caribbean coastal ecosystems. Efficient, large-scale monitoring of *A. palmata* is essential for evaluating restoration success, yet traditional in situ surveys remain costly and spatially constrained. In this study, we acquired high-resolution (1.8 cm) uncrewed aerial vehicle (UAV) imagery of a coral reef within the United States Virgin Islands' (USVI) St. Croix East End Marine Park (STXEEMP) and applied deep learning object detection to identify individual *A. palmata* colonies. We utilized two convolutional neural network architectures, FasterRCNN and MaskRCNN. FasterRCNN was used as an initial screening tool to identify the optimal imagery dataset from several candidates. After identifying the dataset, we used MaskRCNN with an iterative annotation refinement procedure in which initial model predictions were used to augment the training data and achieved an F1 score of 0.78. Detection accuracy was strongly influenced by colony size and apparent water depth, with markedly high accuracy for corals wider than 0.3 m (F1 = 0.87) and located in shallower waters (F1 = 0.81). Beyond detection, MaskRCNN's polygon outputs enabled

Check for updates

Academic Editors: Scot Smith and Kamal Darwish

Received: 15 April 2026
Revised: 19 June 2026
Accepted: 26 June 2026
Published: 1 July 2026

Copyright: © 2026 by the authors. Licensee MDPI, Basel, Switzerland. This article is an open access article distributed under the terms and conditions of the Creative Commons Attribution (CC BY) license.

the measurement of the individual colony area and the generation of high-resolution coral density maps. These products complement broader-scale prediction and mapping approaches and provide fine-scale, management-relevant information. Although this study was conducted at a single reef site during one acquisition period, the results suggest that UAV-based deep learning workflows offer a promising approach for coral reef monitoring that could support restoration assessments and conservation decision-making, pending validation across additional sites, seasons, and environmental conditions.

Keywords: *Acropora palmata*; deep learning; UAV; coral reef monitoring; MaskRCNN; FasterRCNN; object detection; remote sensing; St. Croix

1. Introduction

Coral reefs are increasingly threatened by a combination of interacting stressors, including rising sea temperatures, intensifying storms, sedimentation, and ocean acidification—largely driven by anthropogenic climate change [1,2]. Hughes et al. [3] documented that the intensity and frequency of mass coral bleaching events have increased dramatically over the past three to four decades. Beyond their ecological importance, coral reefs provide substantial socioeconomic value. In 2008, Conservation International [4] estimated the global economic value of coral reefs at USD 29.8 billion, with Caribbean reefs alone contributing USD 3.1–4.6 billion annually through ecosystem services related to tourism, fisheries, coastal protection, biodiversity, and carbon sequestration. Given their dual ecological and socioeconomic significance, coral reefs require effective conservation and management strategies implemented at local to regional scales [3,5,6].

Advances in environmental monitoring technologies, particularly remote sensing and machine learning, are increasingly central to addressing these conservation challenges [7,8]. Advancements in remote sensing have enabled the acquisition of data with higher radiometric and spatial resolution across increasingly large spatial extents [9]. At the same time, machine learning methods provide powerful tools for extracting meaningful patterns from datasets that would otherwise be prohibitively large or complex to analyze manually.

We apply deep learning techniques to detect Elkhorn coral (*Acropora palmata*) (Lamarck, 1816), a keystone reef-building species in the Caribbean [10]. *A. palmata* has been a fundamental contributor in building the region's reef framework over the past 5000 years [11] and continues to support high levels of biodiversity while attenuating wave energy that protect coastlines and adjacent habitats, including seagrass beds and mangroves [10]. The complex branching morphology of *A. palmata* creates structurally diverse habitat that supports a wide range of marine organisms, particularly reef-associated fishes that sustain ecologically and economically important fisheries [12–14]. Few coral species are capable of persisting in the shallow, high-energy environments occupied by Elkhorn coral, and the loss of this species would substantially increase the vulnerability of Caribbean islands to coastal erosion and storm impacts [10]. Figure 1 presents an underwater photograph of an *A. palmata* colony from the study area, illustrating the distinctive branching structure that enables species-level identification using high-resolution UAV imagery.

Despite its historic dominance across reef crests in the Caribbean, widespread bleaching events and outbreaks of white band disease have reduced *A. palmata* populations by more than 90% since 1980 [3,15,16] and in some areas have led to functional extinction. The primary stressors of coral disease, chronic sedimentation, tropical storm damage, and predation continue to threaten the remnant populations [10,17–19]. Due to these severe declines, *A. palmata* was listed as a threatened species under the U.S. Endangered Species

Act in 2006, and NOAA reaffirmed this status in 2014 [19,20]. Despite its imperiled status, *A. palmata* continues to provide critical ecosystem services, contributing to sand generation, fishery productivity, and tourism-based economies [21–23]. In response to ongoing population losses, active restoration efforts have been taking place across the Caribbean. For example, The Nature Conservancy (TNC) has been involved in outplanting *A. palmata* colonies on St. Croix's reefs since 2012, employing a wide range of restoration techniques including microfragmentation and facilitated sexual reproduction [24], aimed at enhancing population recovery and long-term resilience.



Figure 1. Underwater photograph of an *Acropora palmata* (Elkhorn coral) colony in the study area near Teague Bay, St. Croix, USVI. The distinctive branching morphology is clearly visible.

Uncrewed aerial vehicles (UAVs) offer distinct advantages over satellite platforms for coral reef monitoring, including the ability to capture ultra-high spatial resolution imagery at low flight altitudes (e.g., <120 m) while minimizing atmospheric interference and challenges posed by persistent cloud cover, common limitations in the Caribbean region [25,26]. In parallel, the evolution of deep learning, particularly convolutional neural networks (CNNs), has enabled significant progress in automated marine object detection, with successful applications ranging from sea cucumber identification and habitat suitability mapping to coral classification [27–29]. CNNs leverage both geometric and radiometric information through hierarchical feature learning across successive convolution, pooling, and activation layers, allowing objects to be detected at multiple spatial scales [30–33].

Despite these advances, the application of instance segmentation architectures such as MaskRCNN for species-level coral detection using UAV imagery remains underexplored. Earlier work by Kutser and Jupp [34] concluded that spectral data alone were insufficient to reliably classify corals at the species level. By contrast, deep learning models applied to UAV imagery have the potential to integrate both radiometric and geometric information with detailed structural cues, such as colony morphology and spatial context, to improve

the detection and differentiation of visually similar benthic features. This capability is particularly relevant for species such as *A. palmata*, whose branching architecture provides an opportunity for species-level identification at the colony level beyond spectral information alone.

In this study, we evaluated MaskRCNN for detecting individual *A. palmata* colonies from ~1.8 cm resolution UAV orthomosaics collected over a reef in St. Croix East End Marine Park (STXEEMP). We evaluated model performance across varying coral sizes and a depth stratification, implemented an iterative, human-guided annotation refinement strategy to improve MaskRCNN training, and evaluated the added value of polygon-level outputs for generating high-resolution coral density maps for reef monitoring and management.

2. Materials and Methods

2.1. Study Area

Our study area is a coral reef located north of Yellowcliff Bay and Teague Bay along the northeastern coast of St. Croix, U.S. Virgin Islands (Figure 2). The site lies entirely within the St. Croix East End Marine Park (STXEEMP), the first multiuse marine park established in the USVI. STXEEMP protects over 150 km^2 of marine habitat including a large reef ecosystem [14]. Pittman et al. [14] found that Teague Bay had the highest density of hard coral within the park and concluded that runoff from land development and dirt roads in the Yellowcliff Bay watershed poses a "high threat" to six sensitive coral species found there, including *A. palmata*. The study area is designated as a No Take Zone and forms part of an ongoing long-term conservation effort aimed at restoring Elkhorn coral populations in the USVI through active outplanting and facilitated sexual reproduction [24]. The reef supports rich species diversity, including a mixture of branching and mounding corals [14], making it both ecologically important and well suited for evaluating species-level coral detection using UAV imagery.

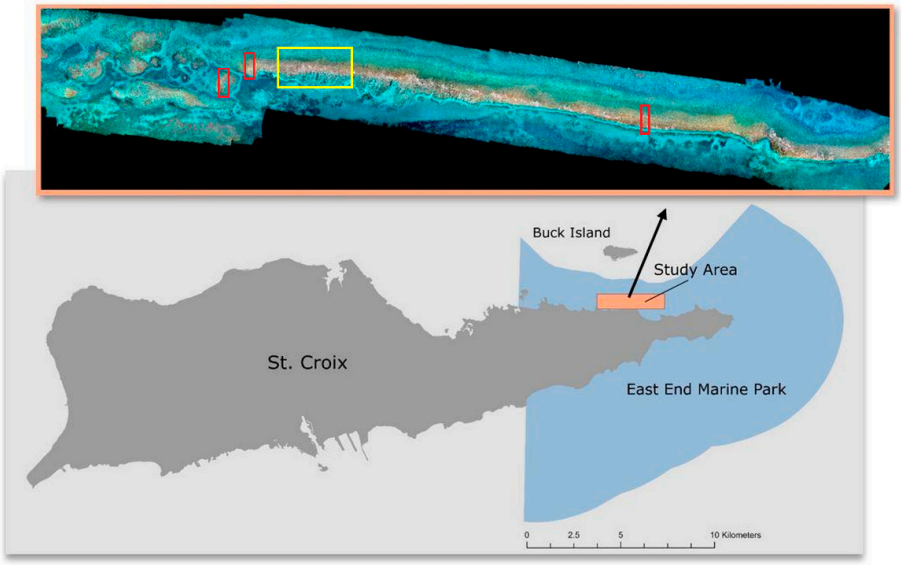


Figure 2. Map of STXEEMP and orthomosaic of the study reef near Teague Bay, St. Croix, USVI, showing boundaries of the marine protected area, the islands of St. Croix and Buck Island, and the study area. The yellow rectangle overlain on the image represents the area from which initial training data were created. The red polygons represent the areas in which the accuracy assessment was conducted.

2.2. Data Acquisition

We acquired imagery of the coral reef using a WingtraOne (Wingtra AG, Zurich, Switzerland) fixed-wing vertical take-off and landing (VTOL) UAV (Figure 3). A total of

ten UAV missions were conducted between 25 May and 2 June 2021, covering 1.48 km^2 at a nominal spatial resolution ranging from 1–1.8 cm, depending on flight altitude. Image acquisition was timed to morning and late afternoon periods when the Sun's angle was less than 45 degrees above the horizon to minimize sun glint on the water surface. In situ validation data were collected concurrently by snorkelers, who captured in-water georeferenced photographs of Elkhorn coral colonies and compiled a point-based spatial database of coral locations. A secondary set of higher-resolution imagery (<1 cm) was collected over a scattered areas within the larger study area (~14 km^2 or ~1% of the primary extent, but focused entirely on the reef itself) using a DJI Phantom 4 quadcopter (DJI, Shenzhen, China). This imagery was collected in order to supplement the in situ data and generate data in areas that were too shallow for snorkelers to visit (Figure 4). Both of these sets of field observations (higher resolution imagery and snorkel points) were used to generate separate sets of training and validation data for model development (Figure 2).



Figure 3. The WingtraOne fixed-wing VTOL UAV used for data collection, shown completing a survey flight over the coral reef near Cramer's Park on the east end of St. Croix.



Figure 4. A secondary set of higher-resolution imagery (<1 cm) was collected over a smaller extent using a DJI Phantom 4 quadcopter UAV at ~30 m above the water. Depicted here is an orthomosaic of those data showing *Acropora palmata* colonies within the study area (golden-orange/brown branching features) visible against the reef substrate.

2.3. Data Processing

The UAV imagery was georeferenced using post-processed kinematic (PPK) corrections. Base station data were obtained from the NOAA/NGS continuously operating reference station (CORS) at the Very Long Baseline Array (VLBA) antenna facility, located within several hundred meters from the UAV launch site (Figure 3). Cloud-based photogrammetry software was used to generate orthomosaics at 1.8 cm spatial resolution and digital surface models (DSMs) at approximately twice that resolution. The orthomosaics and DSMs were resampled to 1 cm resolution and co-registered to ensure consistent cell alignment. These layers were composited into a four-band raster comprising elevation, blue, green, and red channels. Negative elevation values were converted to positive integer depth values to reduce file size and improve the interpretability of the depth data.

We employed a deep learning framework that provides a GIS-based interface with common open-source machine learning implementations, following a three-step workflow consisting of model training, building and execution [35]. All models were trained and executed using the deep learning tools in Esri ArcGIS Pro 3.1, which internally employ PyTorch 1.13 with torchvision as the backend framework. FasterRCNN was trained with a ResNet-50 backbone initialized from ImageNet-pretrained weights (frozen during training), a chip size of 256 pixels, batch size of 4, maximum of 20 epochs with early stopping based on validation loss, and a 10% validation split. MaskRCNN models were trained with chip size 256, batch size 16, maximum of 30 epochs with early stopping monitoring validation loss, 10% validation split, random weight initialization for unfrozen layers, default data augmentation, and a frozen ImageNet-pretrained backbone. Default learning rate schedules were used for both architectures. Training data were generated by manually digitizing polygons around coral colonies identified in the lower-resolution imagery and verified using the higher-resolution imagery (Figure 5). Although the primary objective was to detect *A. palmata*, additional coral species were included in the training dataset to reduce the likelihood of misclassification. For accuracy assessment, point features were created for all coral colonies visible in the high-resolution imagery, each annotated with attributes describing coral type, colony width, and depth derived from the DSM. Critically, the 651 accuracy assessment points were located in spatially distinct sections of the reef, primarily along the edges of the study area, and were entirely separate from the areas used to generate training polygons, which were concentrated toward the middle of the reef. Both assessment and training areas included cross-sections of the fore-reef, reef crest, and back-reef zones and were covered by the higher-resolution DJI Phantom imagery. Only *A. palmata* detections were evaluated for accuracy; the other trained classes served solely to reduce misclassification. A point-in-polygon matching protocol was used for accuracy assessment: a true positive (TP) was recorded when an assessment point fell within a dissolved detection polygon, a false positive (FP) when a detection polygon contained no assessment point, and a false negative (FN) when an assessment point did not fall within any detection polygon.

Deep learning object detection architectures can be broadly categorized by their output type. Semantic segmentation classifies every pixel in an image into categories but does not distinguish individual objects, while instance segmentation identifies and delineates each discrete object separately [32,36]. FasterRCNN [33] is a two-stage object detector that generates region proposals and then classifies each proposal, producing bounding boxes around detected objects. MaskRCNN [36] extends this architecture by adding a parallel branch that predicts a pixel-level segmentation mask for each detected instance, enabling precise delineation of object boundaries. Both architectures use a backbone feature extractor, commonly a residual network (ResNet) [37]. ResNet variants are designated by their layer depth—resnet50, resnet101, and resnet152 contain 50, 101, and 152 convolutional layers,

respectively. While deeper networks can learn more complex features, they also require greater computational resources and larger training datasets and may be more susceptible to overfitting when applied to smaller datasets.

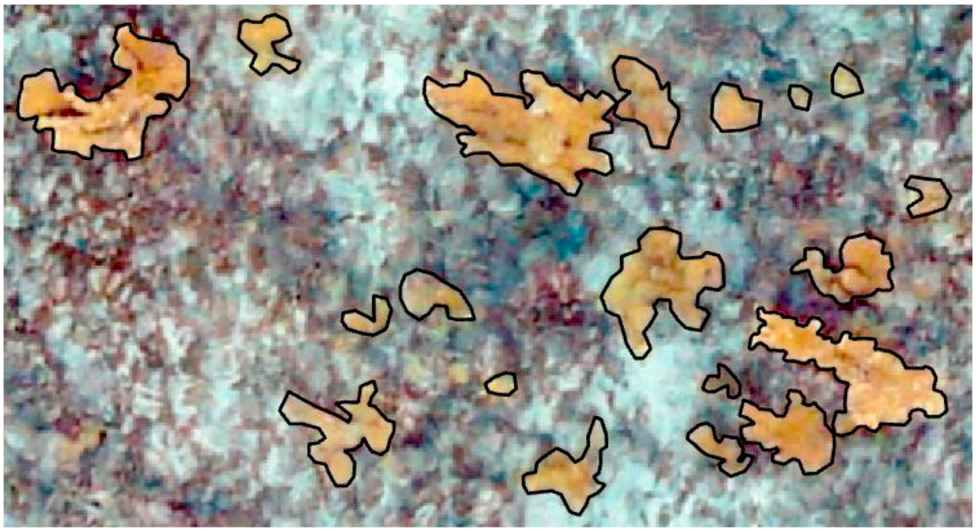
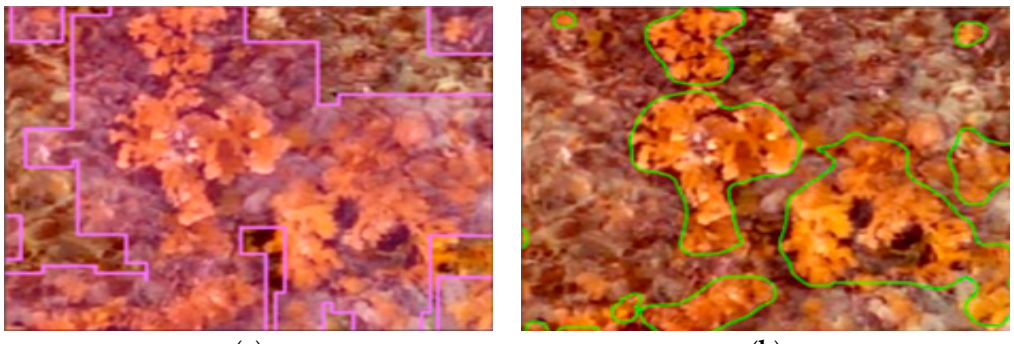


Figure 5. Training data for the deep learning model created by digitizing corals throughout the reef. Each of the polygons (outlined in black) were attributed as *A. palmata*, *A. millepora*, or mounding coral.

We first trained a FasterRCNN model as a rapid screening tool to identify which of the 10 imagery datasets yielded the best detection performance. FasterRCNN produces bounding boxes for each detected instance and was computationally efficient for this initial evaluation. We then trained MaskRCNN models at three layer depth levels: resnet50 (small), resnet101 (medium), and resnet152 (large) using the same training data. Unlike FasterRCNN, MaskRCNN outputs polygons that outline detected features, providing information about colony shape and area (Figure 6). We also implemented an iterative annotation refinement strategy: the output from the initial MaskRCNN resnet101 (medium) model served as a starting point for human annotators, who manually verified each predicted polygon, corrected boundary delineations, deleted false positives, and digitized missed colonies. This process approximately doubled the training area and added roughly 200 additional verified polygons to the original approximately 1500 training polygons in the initial area, yielding approximately 3000 total training polygons across an expanded spatial extent. The refined dataset was then used to retrain MaskRCNN at all three backbone depths. Output polygons from both architectures were dissolved by coral type to prevent overlapping polygons from inflating precision scores. For MaskRCNN outputs, a zonal summary of the DSM was computed within each detected polygon to obtain the mean depth.



(**a**) (**b**)

Figure 6. Each image is at the same resolution and location. (**a**) The dissolved FasterRCNN output (originally rectangles). (**b**) MaskRCNN output with dissolved polygons masks.

2.4. Accuracy Assessment

We used a combination of in situ data gathered by a field team and a secondary set of higher-resolution UAV imagery to conduct accuracy assessments. We determined false positives (*FP*), where the model detected a coral colony that was not confirmed by visual interpretation, and false negatives (*FN*), where a coral colony was identified by a human observer but not detected by the model. We calculated Precision, Recall, and F1 score as defined below:

$$\text{Precision} = \frac{TP}{TP + FP}$$

$$\text{Recall} = \frac{TP}{TP + FN}$$

$$\text{F1 Score} = 2 \times \frac{\text{Precision} \times \text{Recall}}{\text{Precision} + \text{Recall}}$$

These metrics were calculated for each model configuration. The FasterRCNN model was first run on all 10 imagery datasets, and the dataset producing the best F1 score was used for all subsequent analyses. We further binned the accuracy data by coral size (0.10 m width increments from 0–2.50 m) and into two depth categories (shallow reef and deeper reef). The depth categories were delineated spatially in the reference areas using a combination of visual interpretation of the imagery and the photogrammetrically derived DEM (Figure 7). Due to light attenuation and other effects, the exact threshold between these two classes is not known precisely; however, the in situ observation of the reef indicates that it was around 1.5 m (approximate height of a diver positioned vertically in the water column).

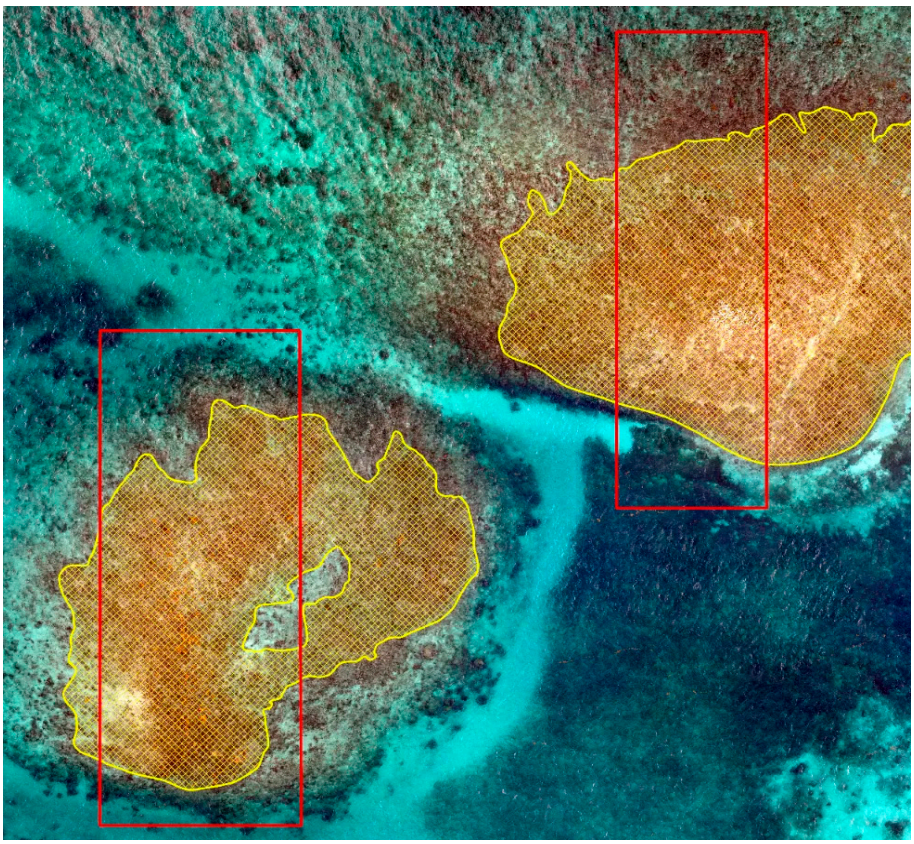


Figure 7. The two westernmost accuracy assessment areas outlined in red (The same that appear in Figure 2) with the "shallow" reef class delineated in yellow. This area was delineated spatially using a combination of visual interpretation of the imagery and the photogrammetrically derived DEM. Accuracy assessment points within this zone were classified as "shallow". Outside this area they were labeled "deeper".

3. Results

3.1. Imagery Assessment

The FasterRCNN model trained on the original data was used to evaluate which of the 10 imagery datasets produced the best results. Imagery captured on 25 May 2021 (75 m altitude, partly cloudy) yielded the highest F1 score of 0.73 (Precision = 0.90, Recall = 0.61), and all further analyses used this dataset (Table 1). Across all datasets, precision scores remained consistently high (minimum 0.84), while recall varied considerably (minimum 0.27). Flight altitude and cloud cover did not exhibit a consistent influence on model performance: the second-best F1 score came from imagery at 120 m in clear skies, while the worst came from 70 m in clear skies. We note that selecting the best-performing dataset for subsequent analyses means the reported MaskRCNN results are conditional on this acquisition and may not represent average operational performance across all imaging conditions.

Table 1. Accuracy scores by imagery dataset.

F1	Recall	Precision	Dataset
0.73	0.61	0.90	**May 25—PM—Partly Cloudy—75 m**
0.63	0.48	0.91	May 26—AM—Clear—75 m
0.70	0.56	0.91	May 27—PM—Clear—75 m
0.70	0.55	0.92	May 27—PM—Clear—90 m
0.66	0.52	0.89	May 28—AM—Mostly Sunny—90 m
0.68	0.57	0.84	May 28—AM—Clear—90 m
0.66	0.51	0.94	May 28—PM—Clear—120 m
0.67	0.53	0.90	May 30—PM—Clear—120 m
0.41	0.27	0.84	May 31—AM—Clear—70 m
0.72	0.58	0.95	June 2—AM—Clear—120 m

Note: Datasets described by collection time, weather conditions, and altitude. All accuracy scores are based on FasterRCNN outputs trained on the same data. Bold row indicates best overall performance.

3.2. Evaluation of MaskRCNN Outputs

When trained on the original annotation dataset, the MaskRCNN models did not produce better F1 scores than the FasterRCNN baseline. The MaskRCNN models achieved precision scores comparable to FasterRCNN, but recall and F1 scores were generally lower (Table 2). However, we then augmented and refined the training data by hand-correcting the output from the initial MaskRCNN resnet101 model, thus creating enhanced training data. The enhanced training data were then refined into another set of training data for the MaskRCNN models. These "refined" models, with roughly twice the amount of augmented training data, then surpassed the accuracy of the FasterRCNN model we had created previously in terms of their F1 scores. The refined resnet50 model achieved the best overall results with an F1 score of 0.78 (Precision = 0.76, Recall = 0.82), demonstrating a substantial improvement in precision over both the original MaskRCNN and FasterRCNN models. Although the difference in accuracy can primarily be attributed to the larger training dataset rather than the architecture itself, the MaskRCNN outputs provide richer information about individual colony size and total coral area because they delineate polygons matching the shape of the detected coral rather than bounding boxes [36].

Table 2. Accuracy scores by model architecture and convolution depth (n = 651).

TP	FP	FN	F1	Recall	Precision	Deep Learning Model
273	11	378	0.59	0.42	0.96	MaskRCNN-resnet50
326	28	325	0.65	0.50	0.92	MaskRCNN-resnet101

Table 2. *Cont.*

TP	FP	FN	F1	Recall	Precision	Deep Learning Model
371	60	280	0.68	0.57	0.86	MaskRCNN-resnet152
534	**169**	**117**	**0.78**	**0.82**	**0.76**	Refined MaskRCNN-resnet50
443	72	208	0.76	0.68	0.86	Refined MaskRCNN-resnet101
404	30	247	0.74	0.62	0.93	Refined MaskRCNN-resnet152
397	44	254	0.73	0.61	0.90	Best F1 FasterRCNN Model

Note: Refined models used human-corrected output from the initial MaskRCNN model as enhanced training data. FasterRCNN was not retrained with the refined dataset and is reported as a baseline. Bold row indicates best overall performance.

3.3. Influence of Coral Size and Depth

Using the outputs from the best-performing model (refined MaskRCNN, resnet50), we examined how coral size and depth influenced detection accuracy. Identified field-sampled corals ranged from 0.08 m to 2.52 m in width. A size threshold emerged at approximately 0.3 m width: recall increased from 0.56 for corals smaller than 0.3 m to 0.89 for corals larger than 0.3 m, and precision improved from 0.49 to 0.84, yielding F1 scores of 0.52 and 0.87, respectively (Figure 8; Table 3).

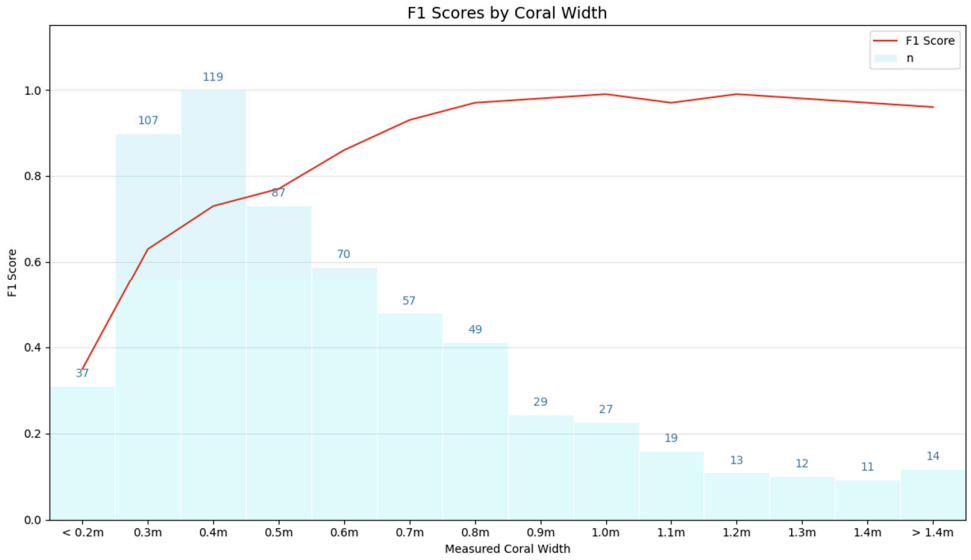


Figure 8. Accuracy (F1) scores (red line) and number (*n*) of field samples (blue bars) for each width group. Groups are organized into 0.1 m bins with the label indicating upper limit and previous label indicating lower limit, except for the first and last labels.

Table 3. Accuracy by coral size and depth thresholds.

n	TP	FP	FN	F1	Recall	Precision	MaskRCNN Refined-Resnet50
144	81	84	63	0.52	0.56	0.49	Size < 0.3 m (0.07 m^2)
507	453	85	54	0.87	0.89	0.84	Size > 0.3 m (0.07 m^2)
597	512	160	85	0.81	0.86	0.76	Shallower Reef
54	22	9	32	0.51	0.40	0.72	Deeper Reef

Note: Accuracy scores for the refined MaskRCNN (resnet50) model showing Precision, Recall, and F1 for above and below thresholds in coral size and water depth.

Apparent water depth had a noticeable influence on accuracy (Table 3). For shallower depths, the F1 score was 0.81, but for deeper areas, that value dropped to 0.51. The change in F1 score was primarily driven by a marked difference in recall (0.86 in shallow water to 0.40 in deeper water). In this dataset, the model appears to underestimate the number of corals in deeper water while still efficiently detecting actual corals.

4. Discussion

4.1. Model Performance and the Iterative Refinement Strategy

Our results demonstrate that MaskRCNN is a viable deep learning approach for detecting *A. palmata* from UAV imagery, achieving an F1 score of 0.78 after iterative annotation refinement. Larger coral colonies over 0.3 m in width were detected with even higher accuracy (0.87). Another finding of this study is that MaskRCNN's performance markedly improved through an annotation refinement strategy in which its initial predictions served as a starting point for human annotators who manually verified, corrected, and supplemented the training polygons across an expanded area. This human-guided refinement resulted in a meaningfully better overall F1 score. The annotation refinement technique effectively leverages MaskRCNN's ability to generate detailed polygon delineations, producing training data that more accurately represents the spatial extent and morphology of individual coral colonies than manually digitized polygons alone.

MaskRCNN offers an advantage over FasterRCNN in that its polygon outputs enable estimation of individual colony area, although polygon accuracy was not independently validated with segmentation-specific metrics in this study. Such estimates are nonetheless valuable for restoration monitoring, where tracking changes in total coral cover and individual colony growth over time is essential. FasterRCNN's bounding boxes, while useful for detection, do not capture colony morphology and, in this case, consistently overestimated coral area. Instance segmentation architectures allow for delineating complex benthic features such as coral colonies.

FasterRCNN was computationally faster, processing the accuracy assessment area in approximately 21 min compared to 24 min for MaskRCNN on an RTX 3090 GPU with 24 GB vRAM, 64 GB RAM, and an i9-12900KF CPU. While this difference was small for our study area, it could be more significant on larger datasets or less powerful hardware.

4.2. Environmental Factors Affecting Detection

Coral size and apparent water depth emerged as important factors influencing detection accuracy. The strong improvement in F1 scores for colonies larger than 0.3 m width indicates that spatial resolution is a primary limiting factor. Coral colonies smaller than 0.3 m width occupy relatively few pixels even at 1.8 cm resolution, likely rendering pattern recognition ineffective. Smaller *A. palmata* colonies would then be difficult for the model to distinguish from surrounding substrate and other similar colored features, but with dissimilar physical structure (e.g., sea fans, sargassum, other orange/brown coral). A sensor capable of higher spatial resolution imagery or flying at a lower altitude would likely improve detection of smaller colonies. However, we hypothesize that at some finer spatial resolution, gains in accuracy scores would be reduced or altogether limited by obscuration due to the optical condition of the environment (mainly the water and the dynamic nature of the environment). These interacting effects warrant further investigation.

The marked decrease in precision at greater depths (approximately 1.5 m) is likely driven by increasing water column effects that degrade image clarity. As depth increases, light attenuation, refraction, and caustic patterns become more pronounced, reducing both spectral and spatial contrast between coral colonies and the surrounding substrate. The model's tendency to miss harder-to-see coral in deeper water suggests this is the case.

We note that the DSM-derived depth values used in this analysis were not systematically and independently validated against in situ bathymetric measurements, and UAV photogrammetry over shallow water is subject to refraction and surface motion effects that may introduce systematic depth errors. The depth-stratified accuracy results reported here should therefore be interpreted with this caveat in mind.

4.3. Sargassum Misidentification

An unexpected source of false positives was the misclassification of *Sargassum*, a common Caribbean macroalga, as *A. palmata* (Figure 9). The similar size, shape, and color of *Sargassum* at the spatial scale of the imagery made it difficult for the model to distinguish from coral colonies. While *Sargassum* contributed only a small number of false positives in our study area, greater prevalence could substantially impact results. Future applications should include *Sargassum* as a training class to reduce this source of confusion, similar to our inclusion of other coral classes (e.g., mounding coral).

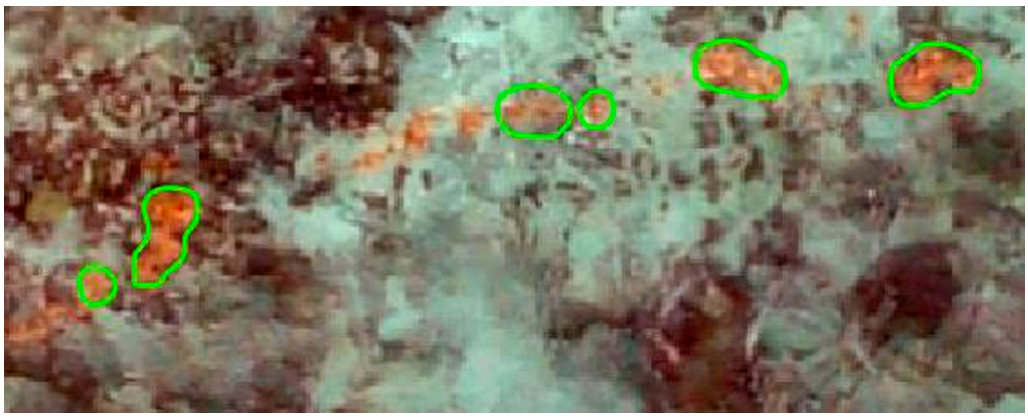


Figure 9. The green outline polygons are examples of those labeled by the machine learning process to be *A. palmata* coral but in this case are incorrect. Because of its similar size, shape, and color at this spatial scale, Sargassum was sometimes incorrectly classified as *A. palmata*. Future applications should include Sargassum as a training class.

4.4. Applications and Broader Impact

Deep learning methods for detecting *A. palmata* from UAV imagery offers a faster alternative to traditional in situ surveys while producing reliable and ecologically meaningful results. These methods can be used to evaluate restoration success, measure coral growth and abundance, assess storm-related damage, and potentially support disease monitoring. High-resolution, drone-derived density maps generated from MaskRCNN outputs (Figure 10) provide a valuable supplement to coarser NOAA prediction products based on environmental covariates such as depth and rugosity (Figure 11). While the NOAA maps predict coral abundance at approximately 20 m cell resolution based on habitat suitability, our approach identifies individual colonies and subsequently aggregates results, preserving fine-scale spatial detail that is lost at coarser resolutions. This capability positions UAV-based deep learning workflows as a critical complement to existing regional-scale monitoring efforts, bridging the gap between broad habitat modeling and site-level ecological assessment.

Monitoring corals at this spatial and temporal scale has the potential to support early detection of disease or other emerging hazards, while also complementing coarser satellite-based observations across multiple spatial scales [26]. Further research is needed to determine which additional sessile organisms, such as sea anemones or additional coral species, can be reliably detected using similar deep learning techniques [27]. Perhaps even more promising is the potential use of UAV-acquired imagery to provide high temporal resolution datasets (e.g., hourly) which could enable monitoring of slower moving but non-sessile organisms in shallow marine environments, such as *Aliger gigas* (Queen Conch).

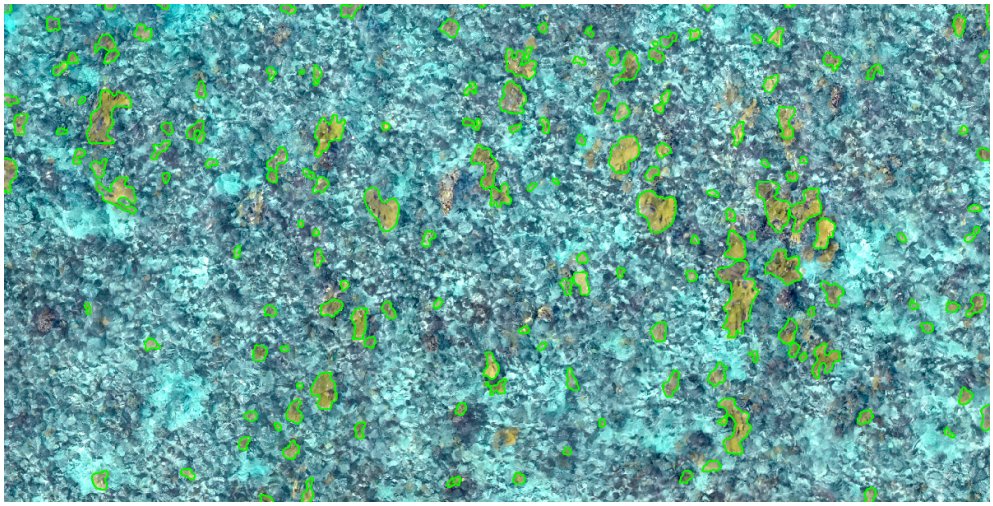


Figure 10. A representative subset of the MaskRCNN output (green polygon outlines) which was created for the entire study area displayed here with the imagery used as input. This output was aggregated into larger cells in the following figure (Figure 11).

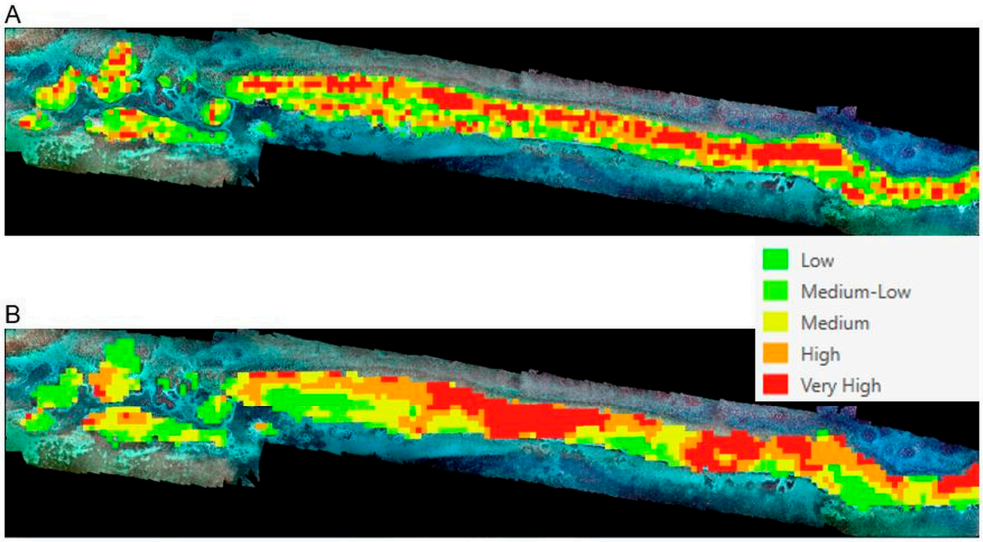


Figure 11. (**A**) Sum of the area covered by *A. palmata* in each cell as detected by the deep learning model, at fine spatial resolution. (**B**) Prediction of coral density based on environmental factors, created by NOAA.

5. Conclusions

Corals provide essential ecological and socioeconomic benefits, and their continued preservation is critical to the well-being of Caribbean communities. A foundational component of effective conservation is robust monitoring, yet traditional survey methods are often costly, logistically challenging, and time-consuming. UAV imagery combined with deep learning techniques provides a faster, more cost-effective approach for coral monitoring, enabling researchers and resource managers to make more timely, data-driven conservation and restoration decisions.

This study demonstrates that MaskRCNN is an effective deep learning method for detecting individual *A. palmata* colonies from UAV imagery, achieving an overall F1 score of 0.78 after iterative annotation refinement. Model performance was further enhanced through an annotation refinement strategy in which initial MaskRCNN outputs were incorporated to enhance training data, resulting in substantial gains in model precision. In addition to improved detection accuracy, MaskRCNN's polygon outputs enabled measure-

ment of individual colony area, an essential capability for coral censusing, density mapping, and restoration monitoring. Detection accuracy was highest for coral colonies larger than 0.3 m in shallower waters (based on apparent depth derived from UAV photogrammetry), suggesting that improvements to sensor spatial resolution and water column correction techniques could further extend the applicability of this approach. The high-resolution coral density maps produced by this workflow provide a critical complement to coarser regional prediction products, offering spatially detailed information that supports more informed, site-level conservation and restoration decision-making.

Author Contributions: Conceptualization, S.W., G.T.R. and S.R.S.; methodology, S.W., G.T.R. and S.R.S.; software, G.T.R.; validation, S.W.; formal analysis, S.W. and G.T.R.; investigation, S.W., G.T.R., and S.R.S.; resources, S.R.S.; data curation, G.T.R. and S.R.S.; writing—original draft preparation, S.W. and G.T.R.; writing—review and editing, G.T.R. and S.R.S.; visualization, S.W. and G.T.R.; supervision, G.T.R. and S.R.S.; project administration, S.R.S. All authors have read and agreed to the published version of the manuscript.

Funding: This work was supported by a grant from The United States Department of Commerce/NOAA to the University of Southern Mississippi (NA19NOS4690205), which funded salary and equipment. The Nature Conservancy provided travel and field support in St. Croix, USVI using funds provided by The National Fish and Wildlife Foundation (NFWF) Coral Reef Conservation Fund.

Data Availability Statement: The UAV imagery and deep learning model outputs presented in this study are available on request from the corresponding author.

Acknowledgments: We are sincerely grateful to The Nature Conservancy's U.S. Virgin Islands team for their assistance with field data collection and interpretation of results, with special thanks to Celeste Jarvis, Jessica Ward, Matthew Davies, Delsabriana Gonzalez, Racquel Maronde, Katie Owens, Mikayla Barnwell, and Lisa Terry. We are particularly thankful to Alexandra Gutting for sharing ancillary data that supported this project. We also thank Gregory Carter for reviewing early drafts and providing valuable guidance on the research design as well as the anonymous reviewers for their constructive and insightful comments.

Conflicts of Interest: The authors declare no conflicts of interest.

References

1. Hoegh-Guldberg, O. Coral Reef Ecosystems and Anthropogenic Climate Change. *Reg. Environ. Change* **2011**, *11*, 215–227. [CrossRef]
2. Rogers, C.S. Responses of Coral Reefs and Reef Organisms to Sedimentation. *Mar. Ecol. Prog. Ser.* **1990**, *62*, 185–202. [CrossRef]
3. Hughes, T.P.; Anderson, K.D.; Connolly, S.R.; Heron, S.F.; Kerry, J.T.; Lough, J.M.; Baird, A.H.; Baum, J.K.; Berumen, M.L.; Bridge, T.C.; et al. Spatial and Temporal Patterns of Mass Bleaching of Corals in the Anthropocene. *Science* **2018**, *359*, 80–83. [CrossRef] [PubMed]
4. Conservation International. *Economic Values of Coral Reefs, Mangroves, and Seagrass: A Global Compilation*; Center for Applied Biodiversity Science, Conservation International: Arlington, VA, USA, 2008.
5. Costanza, R.; de Groot, R.; Sutton, P.; van der Ploeg, S.; Anderson, S.J.; Kubiszewski, I.; Farber, S.; Turner, R.K. Changes in the Global Value of Ecosystem Services. *Glob. Environ. Change* **2014**, *26*, 152–158. [CrossRef]
6. Schill, S.R.; Raber, G.T.; Roberts, J.J.; Treml, E.A.; Brenner, J.; Halpin, P.N. No Reef Is an Island: Integrating Coral Reef Connectivity Data into the Design of Regional-Scale Marine Protected Area Networks. *PLoS ONE* **2015**, *10*, e0144199. [CrossRef] [PubMed]
7. Crisci, C.; Ghattas, B.; Perera, G. A Review of Supervised Machine Learning Algorithms and Their Applications to Ecological Data. *Ecol. Model.* **2012**, *240*, 113–122. [CrossRef]
8. El Mahrad, B.; Newton, A.; Icely, J.; Kacimi, I.; Abalansa, S.; Snoussi, M. Contribution of Remote Sensing Technologies to a Holistic Coastal and Marine Environmental Management Framework: A Review. *Remote Sens.* **2020**, *12*, 2313. [CrossRef]
9. Fallati, L.; Saponari, L.; Savini, A.; Marchese, F.; Corselli, C.; Galli, P. Multi-Temporal UAV Data and Object-Based Image Analysis (OBIA) for Estimation of Substrate Changes in a Post-Bleaching Scenario on a Maldivian Reef. *Remote Sens.* **2020**, *12*, 2093. [CrossRef]
10. NOAA. *Proceedings of the Caribbean Acropora Workshop: Potential Application of the US Endangered Species Act as a Conservation Strategy*; Bruckner, A.W., Ed.; NOAA Technical Memorandum NMFS-OPR-24; NOAA: Silver Spring, MD, USA, 2003; 199p.

11. Gladfelter, E.H.; Monahan, R.K.; Gladfelter, W.B. Growth Rates of Five Reef-Building Corals in the Northeastern Caribbean. *Bull. Mar. Sci.* **1978**, *28*, 728–734.
12. Lirman, D. Reef Fish Communities Associated with *Acropora palmata*: Relationships to Benthic Attributes. *Bull. Mar. Sci.* **1999**, *65*, 235–252.
13. Nagelkerken, I.A.; Nagelkerken, W.P. Loss of Coral Cover and Biodiversity on Shallow Acropora and Millepora Reefs after 31 Years on Curaçao, Netherlands Antilles. *Bull. Mar. Sci.* **2004**, *74*, 213–223.
14. Pittman, S.; Dorfman, D.S.; Hile, S.; Jeffrey, C.F.G.; Edwards, M.A.; Caldow, C. *Land-Sea Characterization of the St. Croix East End Marine Park, U.S. Virgin Islands*; NOAA Technical Memorandum NOS NCCOS 170; NOAA: Silver Spring, MD, USA, 2013.
15. Andres, N.G.; Witman, J.D. Trends in Community Structure on a Jamaican Reef. *Mar. Ecol. Prog. Ser.* **1995**, *118*, 305–310. [CrossRef]
16. Manzello, D.P.; Cunning, R.; Karp, R.F.; Baker, A.C.; Bartels, E.; Bonhag, R.; Borreil, A.; Bourque, A.; Brown, K.T.; Bruckner, A.W.; et al. Heat-Driven Functional Extinction of Caribbean Acropora Corals from Florida's Coral Reef. *Science* **2025**, *390*, 361–366. [CrossRef] [PubMed]
17. Sutherland, K.P.; Porter, J.W.; Torres, C. Disease and Immunity in Caribbean and Indo-Pacific Zooxanthellate Corals. *Mar. Ecol. Prog. Ser.* **2004**, *266*, 273–302. [CrossRef]
18. Aronson, R.B.; Precht, W.F. White-Band Disease and the Changing Face of Caribbean Coral Reefs. *Hydrobiologia* **2001**, *460*, 25–38. [CrossRef]
19. NOAA. *Atlantic Acropora Status Review Document*; Boulon, R., Chiappone, M., Halley, R., Jaap, W., Keller, B., Krucznyski, B., Miller, M., Rogers, C., Eds.; Report to NMFS, Southeast Regional Office; NOAA: Silver Spring, MD, USA, 2005; 152p.
20. NOAA. Elkhorn Coral. Available online: https://www.fisheries.noaa.gov/species/elkhorn-coral (accessed on 12 November 2025).
21. Moberg, F.; Folke, C. Ecological Goods and Services of Coral Reef Ecosystems. *Ecol. Econ.* **1999**, *29*, 215–233. [CrossRef]
22. Mumby, P.J.; Broad, K.; Brumbaugh, D.R.; Dahlgren, C.; Harborne, A.R.; Hastings, A.; Holmes, K.E.; Kappel, C.V.; Micheli, F.; Sanchirico, J.N. Coral Reef Habitats as Surrogates of Species, Ecological Functions, and Ecosystem Services. *Conserv. Biol.* **2008**, *22*, 941–951. [CrossRef] [PubMed]
23. Yee, S.H.; Dittmar, J.A.; Oliver, L.M. Comparison of Methods for Quantifying Reef Ecosystem Services: A Case Study Mapping Services for St. Croix, USVI. *Ecosyst. Serv.* **2014**, *8*, 1–15. [CrossRef]
24. Gutting, A.; Schill, S.R. *Facilitated Sexual Reproduction and Outplanting of Acropora palmata in St. Croix, US Virgin Islands, 2012–2022*; The Nature Conservancy Caribbean Program: Christiansted, VI, USA, 2022.
25. Ma, L.; Li, M.; Tong, L.; Wang, Y.; Cheng, L. Using Unmanned Aerial Vehicle for Remote Sensing Application. In Proceedings of the 2013 21st International Conference on Geoinformatics, Kaifeng, China, 20–22 June 2013; pp. 1–5. [CrossRef]
26. Madin, E.M.; Darling, E.S.; Hardt, M.J. Emerging Technologies and Coral Reef Conservation: Opportunities, Challenges, and Moving Forward. *Front. Mar. Sci.* **2019**, *6*, 727. [CrossRef]
27. Li, J.Y.Q.; Duce, S.; Joyce, K.E.; Xiang, W. SeeCucumbers: Using Deep Learning and Drone Imagery to Detect Sea Cucumbers on Coral Reef Flats. *Drones* **2021**, *5*, 28. [CrossRef]
28. Chirayath, V.; Instrella, R. Fluid Lensing and Machine Learning for Centimeter-Resolution Airborne Assessment of Coral Reefs in American Samoa. *Remote Sens. Environ.* **2019**, *235*, 111475. [CrossRef]
29. da Silveira, C.B.; Strenzel, G.M.; Maida, M.; Gaspar, A.L.; Ferreira, B.P. Coral Reef Mapping with Remote Sensing and Machine Learning: A Nurture and Nature Analysis in Marine Protected Areas. *Remote Sens.* **2021**, *13*, 2907. [CrossRef]
30. Yuan, Q.; Shen, H.; Li, T.; Li, Z.; Li, S.; Jiang, Y.; Xu, H.; Tan, W.; Yang, Q.; Wang, J.; et al. Deep Learning in Environmental Remote Sensing: Achievements and Challenges. *Remote Sens. Environ.* **2020**, *241*, 111716. [CrossRef]
31. LeCun, Y.; Bengio, Y.; Hinton, G. Deep Learning. *Nature* **2015**, *521*, 436–444. [CrossRef] [PubMed]
32. Krizhevsky, A.; Sutskever, I.; Hinton, G.E. ImageNet Classification with Deep Convolutional Neural Networks. *Commun. ACM* **2017**, *60*, 84–90. [CrossRef]
33. Ren, S.; He, K.; Girshick, R.; Sun, J. Faster R-CNN: Towards Real-Time Object Detection with Region Proposal Networks. *IEEE Trans. Pattern Anal. Mach. Intell.* **2017**, *39*, 1137–1149. [CrossRef] [PubMed]
34. Kutser, T.; Jupp, D.L.B. On the Possibility of Mapping Living Corals to the Species Level Based on Their Optical Signatures. *Estuar. Coast. Shelf Sci.* **2006**, *69*, 607–614. [CrossRef]
35. ESRI. How Deep Learning Works in ArcGIS. Available online: https://pro.arcgis.com/en/pro-app/latest/help/analysis/deep-learning/deep-learning-in-arcgis-pro.htm (accessed on 14 March 2026).
36. He, K.; Gkioxari, G.; Dollár, P.; Girshick, R. Mask R-CNN. *IEEE Trans. Pattern Anal. Mach. Intell.* **2020**, *42*, 386–397. [CrossRef] [PubMed]
37. He, K.; Zhang, X.; Ren, S.; Sun, J. Deep Residual Learning for Image Recognition. In Proceedings of the IEEE Conference on Computer Vision and Pattern Recognition (CVPR), Las Vegas, NV, USA, 27–30 June 2016; pp. 770–778. [CrossRef]

Disclaimer/Publisher's Note: The statements, opinions and data contained in all publications are solely those of the individual author(s) and contributor(s) and not of MDPI and/or the editor(s). MDPI and/or the editor(s) disclaim responsibility for any injury to people or property resulting from any ideas, methods, instructions or products referred to in the content.